A Numerical Study of Second-Order Turbulent Moments in the Stably Stratified Nocturnal Boundary Layer

Zhu Ping (朱 平) and *Xu Xiaojing* (许小金)
Beijing Institute of Meteorology
and *Li Xingsheng* (李兴生)
Academy of Meteorological Science, SMA
Received November 9, 1990; revised September 12, 1991

ABSTRACT

The structures and the vertical profiles of turbulent variance and covariance of the stably stratified boundary layer (SBL) are simulated with a second-order closure turbulence model. The results confirm that the vertical profiles of the dimensionless turbulence variance and covariance can be well represented by the form $F = A(1 - Z/h)^{\alpha}$. Here h is the height of SBL, and both exponent α and coefficient A are the functions of terrain, baroclinicity, radiation cooling and the state of temporal development of SBL. Comparing with Minnesota and Cabauw experiment data, we have analysed the value of α and expounded the main reasons that great difference in α exists among different literatures.

I. INTRODUCTION

Although many features of SBL have been further recognized by using some high-order turbulence models for several decades (e.g., Wyngaard, 1975; Brost and Wyngaard, 1978; Andre et al., 1978; Blackadar, 1979; Li et al., 1986), the structure and the vertical variation of the second-order turbulent moments of SBL are still not well understood. The former experimental results were also quite different. Tokyo experiment data (Yamamota et al., 1979, Yokayama, 1979) showed quite scatter, and the results of Minnesota data (Caughey, 1979) were different from those of Cabauw data (Nieuwstadt, 1984) and Oklahoma data (Lenschow et al., 1988). In order to clarify the turbulence structure of SBL, some features of second-order turbulent moments were studied by Nieuwstadt, (1984); Sorbjan (1986), Lasser and Arya (1986) and Li (1989) with the theoretical method and the numerical simulation separately. Although these studies showed some features of the turbulent moments of SBL in some extent, they did not obtain the unified conclusions and could not explain the difference among different experiments. Some results even lead to many disputations.

In fact, the structure of the second-order turbulent moments of the SBL is influenced by many factors. At nighttime the turbulence is often less vigorous. As a result, other effects such as advection, baroclinicity become as, or even more, important as turbulence in causing changes of second-order turbulent moments. Thus their vertical profiles are the function of terrain, baroclinicity, radiation, the state of SBL and some other factors. Because the influence of these factors is rather complicated in the atmospheric boundary layer, we have to study the vertical distribution of the second-order turbulent moments of SBL by numerical simulation. In this work, a second-order closure technique was applied to numerical simulation, and we tried to show why so much difference exists among different experimental results.

II. THE MODEL

We consider an infinite flat but slope (at a small angle β to the horizontal) surface with a uniform roughness z_0. The Boussinesq equations for momentum in x and y directions are:

$$\frac{\partial U}{\partial t} = f(V - V_g) - g\frac{\overline{T'}}{T_0}|\beta|\cos\gamma - \frac{\partial(\overline{w'u'})}{\partial z} \quad , \tag{1}$$

$$\frac{\partial V}{\partial t} = -f(U - U_g) + g\frac{\overline{T'}}{T_0}|\beta|\sin\gamma - \frac{\partial(\overline{w'v'})}{\partial z} \quad . \tag{2}$$

Here γ is the angle between the x axis and the fall-line vector (the vector is perpendicular to the contour lines and points down the slope). T_0 denotes the temperature for an undisturbed, adiabatic atmosphere. $\overline{T'}$ is the deviation of temperature from T_0. U_g and V_g are the geostrophic wind components in x and y directions separately. In this study, we consider the simple case that the baroclinicity is caused by the horizontal temperature gradients, the relationship between $\partial\overrightarrow{V_g}/\partial z$ and $\overrightarrow{\nabla_h T}$ is

$$\frac{\partial\overrightarrow{V_g}}{\partial z} = -\frac{g}{fT} \cdot \overrightarrow{\nabla_h T} \times \vec{k} \quad . \tag{3}$$

The equation for mean potential temperature is

$$\frac{\partial\Theta}{\partial t} = -U\frac{\partial\Theta}{\partial x} - \frac{\partial z(\overline{w'\theta'})}{\partial z} + \frac{1}{\rho c_p}\frac{\partial F_N}{\partial z} \quad . \tag{4}$$

Here, in the right side of Eq.(4) the first term denotes horizontal advection. We can consider the influence of baroclinicity through this term. The third term is the net radiative flux divergence, which is an important cooling term at nighttime under clear skies. In this study, the emissivity approximation is used to calculate longwave radiation flux, which, is described in detail in Garratt Brost (1981). The values of emissivity for water vapor used here were suggested by Atwater (1974).

The mean moisture equation is

$$\frac{\partial q}{\partial t} = -\frac{\partial(\overline{w'q'})}{\partial z} \tag{5}$$

Over the slope terrain, the equations of turbulence moments are:

$$\begin{aligned}\frac{\partial\overline{u'_i u'_l}}{\partial t} = {} & U_j\frac{\partial\overline{u'_i u'_j}}{\partial x_j} - \left[\overline{u'_k u'_j}\frac{\partial U_i}{\partial x_j} + \overline{u'_i u'_j}\frac{\partial U_k}{\partial x_j}\right] - \frac{\partial(\overline{u'_i u'_j u'_k})}{\partial x_j} \\ & - \frac{1}{\rho}\left[\overline{u'_k\frac{\partial p'}{\partial x_i}} + \overline{u'_i\frac{\partial p'}{\partial x_k}}\right] + \nu\left[\overline{u'_k\frac{\partial^2 u'_i}{\partial x_j^2}} + \overline{u'_i\frac{\partial^2 u'_k}{\partial x_j^2}}\right] - 2\Omega_j[\varepsilon_{ijl}\overline{u'_k u'_l} + \varepsilon_{kjl}\overline{u'_i u'_l}] \\ & + \frac{\mathbf{g}}{\Theta}[\overline{\theta'\mathbf{u}'_k}(\beta\delta_{i1} + \beta\delta_{i2} + \cos\beta\delta_{i3})(-\cos\gamma\delta_{i1} + \sin\gamma\delta_{i2} + \delta_{i3}) \\ & + \overline{\mathbf{u}'_i\theta'}(\beta\delta_{k1} + \beta\delta_{R2} + \cos\beta\delta_{R3})(-\cos\gamma\delta_{R1} + \sin\gamma\delta_{k2} + \delta_{k3})] \quad ,\end{aligned} \tag{6}$$

$$\begin{aligned}\frac{\partial\overline{u'_j\theta'}}{\partial t} = {} & -U_j\frac{\partial\overline{u'\theta'}}{\partial x_j} - \left[\overline{u'_i u'_j}\frac{\partial\Theta}{\partial x_j} + \overline{u'_j\theta'}\frac{\partial U_i}{\partial x_j}\right] \\ & - \frac{\partial(\overline{u'_i u'_j\theta'})\partial x_j}{} + \frac{1}{\rho}\overline{\theta'\frac{\partial p'}{\partial x_i}} + \left[\overline{\nu\theta'\frac{\partial^2 u'_i}{\partial x_j^2}} + \overline{k u'_i\frac{\partial^2\theta'}{\partial x_j^2}}\right] - 2\Omega_j\varepsilon_{ilk}\overline{u'_k\theta'}\end{aligned}$$

$$+\frac{\mathbf{g}}{\Theta}\theta'^2(\beta\delta_{11}+\beta\delta_{12}+\mathbf{cos}\beta\delta_{13})(-\mathbf{cos}\gamma\delta_{11}+\mathbf{sin}\gamma\delta_{12}+\delta_{13}) \quad . \tag{7}$$

$$\frac{1}{2}\frac{\overline{\partial\theta'^2}}{\partial t}=-\frac{1}{2}\overline{u'_i\frac{\partial\theta'^2}{\partial x_i}}-\overline{u'_i\theta'}\frac{\partial\Theta}{\partial x_i}-\frac{1}{2}\frac{\partial\overline{u'_i\theta'^2}}{\partial x_i}-k\overline{\left(\frac{\partial\theta'}{\partial x_i}\right)^2} \quad . \tag{8}$$

Here, $\nu=\mu/\rho$, μ is the dynamic viscosity. κ is the thermal conductivity. $\mathbf{\Omega}_j$ is the angular vector of the earth's ratation. The terms expressed with black letters result from slope terrain. It is well-known that terrain slope can influence the nocturnal atmospheric boundary layer evolution as it creates a drainage acceleration. For the turbulent variance and covariance equations (6), (7), (8), however, the terms caused by slope terrain are not significant when compared to the others. It can be seen easily through scale analysis of the equations. For example, in Eq.(6), the order of the shear production terms $(\overline{u'_iu'_j}\,\partial U_k/\partial x_j)$ is $[u_*^2\,U_h/h]$, where h is the depth of SBL, and U_h is the value of wind at h. The order of the term caused by slope terrain is $[\frac{g}{\Theta}\,u_*\,T_*\,\beta]$. Taking $\Theta=300$ K, $g=10$ m/s^2, $U_h=10$ m/s, $h=100$ m, $u_*=0.1$ m/s, $T_*=0.1$ K, $\beta=5\times10^{-3}$, we got $[u_*^2\,U_h/h]/[\frac{g}{\Theta}u_*\,T_*\,\beta]=600$. This indicates that for a slight slope the influence of terrain is rather small compared with the shear production term. So, we can then ignore the terms caused by slope and use the turbulent variance and covariance equations of flat terrain as a substitute for the slope condition.

For stable conditions, according to Wyngaard (1975), Brost & Wyngaard (1978), and Nieuwstadt (1984) the second-order equations can be simplified as:

$$0=\left(-\overline{w'u'}\frac{\partial U}{\partial z}-\overline{w'v'}\frac{\partial V}{\partial z}\right)+\frac{g}{\Theta}\overline{w'\theta'}-C_\varepsilon\frac{\bar{e}^3}{l} \quad , \tag{9}$$

$$0=\frac{2}{3}C^2\left(-\overline{w'u'}\frac{\partial U}{\partial z}-\overline{w'v'}\frac{\partial V}{\partial z}\right)+\left(2+\frac{4}{3}C_3\right)\frac{g}{\Theta}\cdot\overline{w'\theta'}-\frac{2}{3}C_\varepsilon\frac{\bar{e}^3}{l}-CC_\varepsilon\frac{\bar{e}}{l}\left(\overline{w'^2}-\frac{\bar{e}^2}{3}\right) \quad , \tag{10}$$

$$0=\left[(1-C_2)\overline{w'^2}-\frac{C_1}{2}\bar{e}^2\right]\frac{\partial U}{\partial z}-(1+C_3)\frac{g}{\Theta}\overline{u'\theta'}+CC_\varepsilon\frac{\bar{e}}{l}\cdot\overline{w'u'} \quad , \tag{11}$$

$$0=\left[(1-C_2)\overline{w'^2}-\frac{C_1}{2}\bar{e}^2\right]\frac{\partial V}{\partial z}-(1+C_3)\frac{g}{\Theta}\overline{v'\theta'}+CC_\varepsilon\frac{\bar{e}}{l}\cdot\overline{w'v'} \quad , \tag{12}$$

$$0=-\overline{w'\theta'}\frac{\partial\Theta}{\partial z}+(1-a_1)\frac{g}{\Theta}\cdot\overline{\theta'^2}-dC_\varepsilon\frac{\bar{e}}{l}\overline{w'\theta'} \quad , \tag{13}$$

$$0=-\overline{w'\theta'}\frac{\partial\Theta}{\partial z}-C_\varepsilon C_\theta\frac{\bar{e}}{l}\cdot\overline{\theta'^2} \quad , \tag{14}$$

$$0=-\overline{w'u'}\frac{\partial\Theta}{\partial z}-(1+a_2)\overline{w'\theta'}\frac{\partial U}{\partial z}-dC_\varepsilon\frac{\bar{e}}{l}\cdot\overline{u'\theta'} \quad , \tag{15}$$

$$0=-\overline{w'v'}\frac{\partial\Theta}{\partial z}-(1+a_2)\overline{w'\theta'}\frac{\partial V}{\partial z}-dC_\varepsilon\frac{\bar{e}}{l}\overline{v'\theta'} \quad . \tag{16}$$

Here, taking

$$C_1=0.207,\quad C_2=0.45,\quad C_3=0.14,\quad C=2.7,$$
$$C_\varepsilon=0.139,\quad C_\theta=1.4,\quad a_2=-0.5,\quad d=9.7,$$
$$a_1=\begin{cases}0.5+1.5Ri^2-Ri^3\ , & 0<Ri<1\\ 1\ . & Ri>1\end{cases}$$

where Ri is the gradient Richardson number; $\overline{e^2}$, $\overline{w'^2}$ and $\overline{\theta'^2}$ are the total turbulent kinetic energy, the vertical velocity variance and the temperature variance respectively.

The characteristic turbulence integral scale can be parameterized as $l = z(1 + z / l_B)^{-1}$. Where $l_B^2 = C_B \overline{w'^2} / \frac{g}{\Theta}\frac{\partial \Theta}{\partial z}$. l_B is called characteristic buoyant force scale. $C_B = 1.69$.

In order to reveal the turbulent structure of SBL, we use two different lower boundary conditions on the potential temperature.

The first is to introduce a surface energy budget on the ground:

$$C_g \frac{\partial \Theta}{\partial t} = R_n - H_m - H_g - E \ . \tag{17}$$

where C_g is heat capacity per unit area of the soil slab, Θ_g is potential temperature of the earth's surface. H_g is the surface turbulent sensible heat flux, E is the surface turbulent latent heat flux, H_m is the ground heat flux at the surface, which can be determined by

$$H_m = \mathrm{kmg} Cg (Tg - Tm) \ , \tag{18}$$

where kmg is the heat transfer coefficient expressed as $\mathrm{kmg} = 1.18\omega$, $\omega = 7.27 \times 10^{-5} \mathrm{s}^{-1}$. T_m is the temperature of soil and independent of time. T_g is the ground temperature.

$$R_n = F^{\downarrow}(0) - C_g \alpha T_g^4 \ . \tag{19}$$

$F^{\downarrow}(0)$ represents downward radiation flux at the surface. α is the Stefan–Boltzmann constant.

The second boundary condition on the potential temperature is to provide a constant cooling rate at surface, i.e. $\partial T_g / \partial t = \mathrm{const}$. One significant advantage of this boundary condition is that the simulated SBL can approach a quasi–steady–state with time.

The other upper and lower boundary conditions are taken as

$$\left.\begin{array}{l} U = Ug, \quad V = 0 \\ \dfrac{\partial \Theta}{\partial z} = 0.35 \quad (\mathrm{K} / 100\ \mathrm{m}) \\ \dfrac{\partial q}{\partial z} = \alpha_q \end{array}\right\} \text{ at } \ z = 2000(\mathrm{m}) \ , \qquad \left.\begin{array}{l} U = V = 0 \\ q = A_s \cdot q_s \end{array}\right\} \text{ at } \ z = z_0$$

where α_q and A_s are constants and q_s is the saturation mixing ratio of the earth's surface. We take the neutral steady–state solution as the initial conditions, and the model prediction runs from 18:00 (local time just as the sunset) till 6:00 the next morning.

A staggered grid scheme is used in the vertical direction. The vertical grid is equally spaced in the transformed variable η, expressed as

$$\eta = Z_i / A_1 + \ln(Z_i + A_2) / A_2) \ .$$

Here $A_1 = 250$, $A_2 = 3.2$, the total vertical grids are 46, and

$$Z_{i-\frac{1}{2}} = \frac{1}{2}(Z_i + Z_{i-1}) \ .$$

All the time–dependent variables (U, V, Θ, q) are defined at Z_i. All the diagnostic quantities, such as Richardson number R_i, the eddy exchange coefficient, $\overline{w'\theta'}$ etc. are defined at $Z_{i-\frac{1}{2}}$.

An implicit diffusion scheme (Richtmyer 1957) is utilized for all the predicted equations.

In our model, We take $z_0 = 0.01$ m, $U_g = 10$ m / s. and $V_g = 0.0$m / s. For the baroclinic condition we modify the geostrophic wind according to Eq.(3) with supposed value of $\partial \Theta / \partial x$.

III. RESULT AND ANALYSIS

The result of our numerical simulation indicates that in the SBL all dimensionless turbulence variances and covariances can simply be represented as

$$\frac{\overline{w'\theta'}}{(\overline{w'\theta'})_0} = \left(1-\frac{z}{h}\right)^{\alpha_1}, \tag{20}$$

$$\frac{\tau}{\tau_0} = \left(1-\frac{z}{h}\right)^{\alpha_2} \tag{21}$$

$$\frac{\overline{e}^2}{u_*^2} = A_e\left(1-\frac{z}{h}\right)^{\alpha_e}, \tag{22}$$

$$\frac{\overline{w'^2}}{u_*^2} = A_w\left(1-\frac{z}{h}\right)^{\alpha_w}, \tag{23}$$

$$\frac{\overline{\theta'^2}}{T_*^2} = A_\theta\left(1-\frac{z}{h}\right)^{\alpha_\theta}. \tag{24}$$

These equations are consistent with the conclusions of Caughey et al.(1979); Nieuwstadt, (1984); Lascer and Arya (1986); and Lenschow et al. (1989). Here, τ is turbulent flux of momentum. $\tau=(\overline{w'u'}^2+\overline{w'v'}^2)^{1/2}$. The subscript "$_0$" denotes the values at the surface. The depth of SBL h is defined as the height at which the vertical turbulent stress falls to 5% of its surface value. Nevertheless because the resolution of the grid is not sufficient, we use cubic-spline interpolation method to determine the value of h. u_* is the friction velocity, and T_* is the temperature scale. All parameters $\alpha_1,\alpha_2,\alpha_e$ etc. can be determined with our simulation results from least-square fitting. In the noctural boundary layer, these parameters depend on the state of development of SBL, terrain, baroclinicity and radiation. In the following sections, we will discuss how these factors influence the vertical distribution of the second-order turbulent moments and the variation of these parameters.

(1) *Radiative cooling at surface*

Radiative cooling of the surface is a major factor that causes the formation and evolution of SBL. In this study two different surface cooling rates are used to simulate the formation and evolution of SBL. First, we study the situation that the surface cooling rate is constant. Brost & Wyngaard (1978) pointed out that the SBL could approach the quasi-steady-state in this case. Our numerical simulation also obtains the same results, and further reveals that if the surface cooling rate is constant, SBL will almost become time-independent after several hours. In addition, it takes shorter time to reach the quasi-steady-state for a larger cooling rate.

Table 1 lists the value of each parameter for second-order turbulent moments when SBL is in the quasi-steady-state for the different surface cooling rates.

Table 1. Parameters for Different Surface Cooling Rate

para / $\partial T_g/\partial t$	α_1	α_2	α_e	α_w	α_θ	A_e	A_w	A_θ
−0.5 Kh^{-1}	1.08	1.69	1.50	1.43	1.49	7.51	1.74	9.03
−1.0 Kh^{-1}	1.06	1.63	1.47	1.39	1.45	7.52	1.73	9.72
−2.0 Kh^{-1}	1.05	1.60	1.42	1.35	1.41	7.54	1.71	10.38

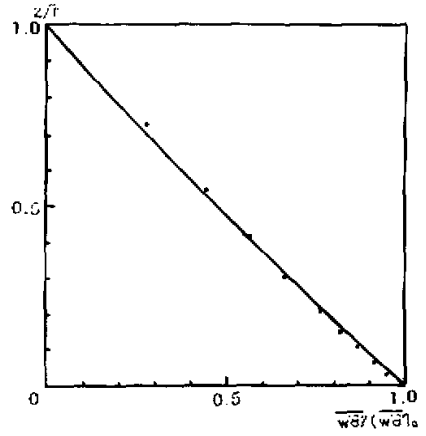

Fig.1. The normalized heat flux as a function of Z / h when $\partial T_g / \partial t = -1.0$ Kh^{-1}. Dots represent the simulated results of our model.

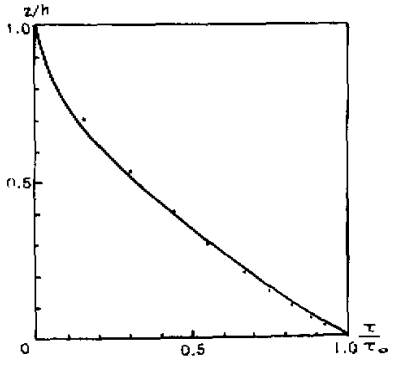

Fig.2. The normalized momentum flux as a function of Z / h when $\partial T_g / \partial t = -1.0$ Kh^{-1}. Dots represent the simulated results of our model.

Fig.1 shows the normalized heat flux as a function of Z / h when the surface cooling rate $\partial T_g / \partial t = -1.0$ Kh^{-1}. Table 1 and Fig.1 indicate that the exponent α_1 is close to 1 regardless of the cooling rate if SBL approaches the "quasi-steady-state". The $\overline{w'\theta'}$ profiles approximately take a linear variation and have a small curvature. This shows that the $\overline{w'\theta'}$ profiles have little relationship with the surface radiation cooling when the quasi-steady-state condition is satisfied. In fact, in the quasi-steady-state, the turbulence production is balanced by the turbulence dissipation. It is this equilibrium that leads to the linear variation of the $\overline{w'\theta'}$ profiles. In this case, the distribution of $\overline{w'\theta'}$ is mainly determinated by turbulence itself instead of external factor. Nieuwstadt (1984) also obtained the results by using the Local Similarity Theory.

Fig.2 illustrates the normalized momentum flux as a function of Z / h when the surface cooling rate $\partial T_g / \partial t = -1.0$ Kh^{-1}. The Cabauw data show that α_2 is about 1.5, which is consistent with our numerical simulation. From Table 1, we note that α_1, α_2, α_e, α_w and α_θ are not very sensitive to surface cooling rate when SBL in the quasi-steady-state. These results are quite similar to the numerical simulation by Lacser & Arya (1986). The values of A_e and A_w are almost constant, while A_θ increases a little when surface radiative cooling increases.

For comparing, the constant surface cooling rate is replaced by the surface energy budget equation to be the lower boundary condition for potential temperature to simulate the evolution of SBL. In this case, the surface cooling rate is time-dependent. The surface temperature decreases rapidly during the first two hours after the sunset. Above the surface, the temperature of atmosphere decreases much more slowly. This results in the surface inversions but with a deep residual layer about it, and the SBL becomes deeper with time.

Table 2 lists the values of all parameters for second-order turbulent moments at different time. It shows that in the first several hours, α_1 is far greater than 1, and later α_1 approaches 1. Caughey (1979) gave $\alpha_1 = 2.50$ from Minnesota data, and Nieuwstadt (1984) obtained $\alpha_1 = 1$ from Cabauw data. From the simulation of our model, we can conjecture the

main reason of the difference between the two experiments is that Minnesota experiment data were observed in the evening transition shortly after the sunset, while Cabauw experiment was carried out in the early morning (a few hours before the sun rises), In the former case, SBL is far from stationary, while in the latter, SBL is evolved fully and the quasi–steady–state condition is almost satisfied. Our simulation results also indicate that the stronger the non–steady–state of SBL, the farther α_1 deviates from 1. Nevertheless, because the characteristic time scale of turbulence field is much smaller than that of mean wind and temperature fields, the suitable range of $\alpha_1 = 1$ is quite wide except the initial developing stage of SBL. By this fact, we may conclude that the development of SBL is very important to the vertical distribution of second–order turbulent moments, and this may be a good reason to explain why the results from Minnesota and Cabauw experiments show so great difference.

Table 2. The Parameters Varying with Time

t \ para	α_1	α_2	α_e	α_w	α_θ	A_e	A_w	A_θ
19:00	2.41	2.25	2.09	1.93	1.74	7.57	1.71	8.35
21:00	1.95	1.97	1.78	1.62	1.59	7.50	1.71	8.92
00:00	1.33	1.76	1.69	1.50	1.52	7.35	1.70	9.35
03:00	1.10	1.63	1.59	1.41	1.48	7.35	1.70	9.74
06:00	0.97	1.56	1.48	1.32	1.44	7.33	1.70	10.01

Now, we consider the mean potential temperature equation

$$\frac{\partial \Theta}{\partial t} = -\frac{\partial \overline{w'\theta'}}{\partial z} \quad . \tag{25}$$

By differentiation, we have,

$$\frac{\partial\left(\frac{\partial \Theta}{\partial z}\right)}{\partial t} = -\frac{\partial^2 \overline{w'\theta'}}{\partial z^2} \quad . \tag{26}$$

In the quasi–steady–state condition, $\partial\Theta / \partial z$ is independent of time (Brost & Wyngaard, 1978; Nieuwstadt, 1984). If we introduce the dimensionless variables:

$$F = \frac{\overline{w'\theta'}}{(\overline{w'\theta'})_0} \quad , \qquad \zeta = z / h \quad ,$$

Eq.(26) becomes

$$\frac{d^2 F}{d\zeta^2} = 0 \quad . \tag{27}$$

With the boundary condition

$$F = 1 \quad \text{for} \quad \zeta = 0; \qquad F = 0 \quad \text{for} \quad \zeta = 1$$

the solution of (27) is

$$\frac{\overline{w'\theta'}}{(\overline{w'\theta'})} = 1 - \zeta \quad .$$

This result was obtained first by Nieuwstadt in 1984. If the quasi–steady–state condition is not satisfied, $\partial\Theta / \partial z$ is the function of time. After the sunset, $\frac{\partial}{\partial t}\left(\frac{\partial \Theta}{\partial z}\right) > 0$. From Eq.(26), we obtain

$$\frac{d^2 F}{d\zeta^2} > 0 \quad .$$

This means the profiles of $\overline{w'\theta'}/(\overline{w'\theta'})_0$ have a curvature. From Eq.(20), we can easily seen that $\alpha_1 > 1$ and the larger value of $d^2F/d\zeta^2$, the larger α_1.

From Table 2, we can also see that α_2 changes considerably wite time. The Minnesota data indicate $\alpha_2 = 2.0$. This is consistent well with our simulation result at 20:00. The distribution exponents α_e, α_w and α_θ and are different at different time. These changes with time indicate that the temporal development state of SBL can also lead to the different vertical distributions of $\overline{e}^2$, $\overline{w'^2}$ and $\overline{\theta'^2}$.

Comparing α_1 with α_2 in Table 2, we find that during the transition (1–2 hours after the sunset) α_1 is larger than α_2 due to rapid development of SBL. This result is consistent with the Minnesota data. When SBL approaches steady–state, α_1 is smaller than α_2. This result is confirmed by Cabauw experiment. Therefore, we can get such conclusions that the relationship between α_1 and α_2 also depends on the development state of SBL.

(2) *Terrain*

For simplicity and remaining the nature of the problem, we take $\gamma = 0$ i.e. assume that the x axis is along the downslope. In order to isolate the influence of terrain, we also do not take the influence of non–steady–state of SBL into consideration. Instead, we only study the case that the lower boundary condition for the potential temperature is provided by a constant surface cooling rate when SBL approaches quasi–steady–state. Taking $\partial T_g/\partial t = 1.0\ \mathrm{Kh}^{-1}$, and assuming other values are the same as those given before, the simulation runs with the slope of 0.001, 0.003, 0.005.

Table 3 lists all characteristic parameters with different slopes of 0.001, 0.003, 0.005.Under this situation, we find that α_1 is smaller than 1. The larger the slope, the smaller the value of $\alpha_1, \alpha_2, \alpha_e$ and α_w. This indicates that the changes of $\overline{w'\theta'}$, τ, $\overline{e}^2$ and $\overline{w'^2}$ in the lower part of SBL in the terrain slope are smaller than those in the flat terrain, while in the upper part of SBL the changes in the terrain slope are larger than those in the flat terrain.

Comparing α_1 with α_2, we see that the changes of τ/τ_0 with slope are larger than those of $\overline{w'\theta'}/(\overline{w'\theta'})_0$. This result indcates that the influence of terrain upon turbulent flux of momentum is larger than that upon turbulent flux of heat.

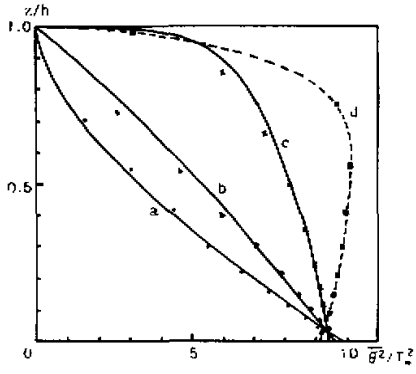

Fig.3. The normalized temperature variance as a function of z/h. "●", "▲", "×", "■" reperesent the simulated results of our model. a: $\beta = 0.0000$, b: $\beta = 0.001$, c: $\beta = 0.003$, d: $\beta = 0.005$.

One significant phenomenon that attracts our attention is the vertical distribution of $\overline{\theta'^2}$ of SBL. Fig.3 shows the nomalized temperature variance as a function of Z/h, we note that the profiles of $\overline{\theta'^2}/T_*^2$ change considerably under different terrain slopes. Particularly, in the case with the slope of 0.005, $\overline{\theta'^2}$ increases with height in the lower part of SBL. Nieuwstadt also discovered this phenomenon when he analysed the structure of θ'^2 with the nonfiltered Cabauw data in 1984. He suggested that it was the low frequency fluctuation that contributes to the temperature variance. This low frequency fluctuation may be caused by some other physical processes such as advection or possibly gravitational wave rather than turbulence. We can imagine that our simulated results are also influences by low frequency. But in our study, the low frequency fluctuation is not stimulated by advection or gravitational wave. We suggest that it would be the drainage wind that causes the low frequency fluctuation. This indicates the terrain can stimulate low frequency fluctuation which has a great influence upon the distribution of the temperature variance.

Table 3. The Parameters at Different Slopes in the Quasi-Steady-State

β \ para	α_1	α_2	α_e	α_w	α_θ	A_e	A_w	A_θ
0.000	1.06	1.63	1.47	1.39	1.47	7.52	1.73	9.72
0.001	0.99	1.36	1.19	1.19	0.87	7.51	1.73	9.61
0.003	0.91	1.09	0.96	0.98	0.20	7.51	1.74	9.39
0.005	0.84	0.89	0.84	0.86		7.51	1.74	9.12

(3) *Baroclinicity*

In general, the atmospheric baroclinicity results from the horizontal temperature gradient. Here, assume that the direction of the horizontal temperature gradient is along the x axis, and $\partial\Theta/\partial x$ equals 2, 5, 8, 10, -8 K / 1000 km respectively. Following Eq.(3), the horizontal temperature gradient of $\partial\Theta/\partial x$ will cause the vertical change of the geostrophic wind. In this study $U_g = 10$ m/s. Therefore, if the direction of horizontal temperature gradient is along the x axis, the geostrophic wind revolves counterclockwise with height. We define it as a cool advection. While, if the direction of $\partial\Theta/\partial x$ is opposite to the x axis, the geostrophic wind will rotate clockwise with height. We call it warm advection. In order to compare with the previous simulation, the surface cooling rate is also taken -1.0 Kh^{-1}. We study the influence of baroclinicity when SBL approaches quasi-steady-state. Table 4 lists all characteristic parameters for second-order turbulent moments with the different horizontal temperature gradients.

It shows that the baroclinicity caused by cool advection makes α_1 and α_2 larger than that under the barotropic condition. The stronger the advection, the larger α_1 and α_2. On the contrary, the warm advection causes α_1 and α_2 to decrease, which means the stronger the advection the smaller α_1 and α_2. Therefore, the two different advections make the turbulent fluxes of heat and momentum change quite differently. The cool advection increase the changes of the turbulent fluxes of heat and momentum in the lower part of SBL, while the warm advection reduces the corresponding changes.

From Table 4, we also find that A_e, A_w and A_θ vary slightly with the different values of $\partial\Theta/\partial x$. The variations of α_e, α_w and α_θ indicate that baroclincity can influence the

vertical distributions of $\overline{e^2}$, $\overline{w'^2}$ and $\overline{\theta'^2}$ of SBL to some extent. The cool advection makes α_e, α_w and α_θ larger and the warm advection makes these parameters smaller.

Table 4. The Parameters for Different $\partial\Theta / \partial x$ in the Quasi-Steady-State

para / $\partial\Theta / \partial x$	α_1	α_2	α_e	α_w	α_θ	A_e	A_w	A_θ
$-8.0\ k / 10^3$ km	0.90	1.43	1.23	1.22	1.21	7.52	1.72	9.87
0.0	1.06	1.63	1.47	1.39	1.47	7.52	1.73	9.72
2.0	1.11	1.67	1.52	1.42	1.67	7.52	1.73	9.71
5.0	1.17	1.70	1.59	1.48	1.83	7.52	1.73	9.70
8.0	1.21	1.78	1.67	1.03	2.04	7.51	1.73	9.65
10.0	1.29	1.85	1.75	1.59	2.19	7.51	1.73	9.61

(4) *Long wave radiation cooling of nocturnal atmosphere*

Let's consider the flat, barotropic situation, and presume the atmosphere be not saturated (i.e., during the evolution of SBL, we do not consider the moisture condensation.) Taking two initial states:

A: $\Theta = \Theta_0 = 290\text{K}$

$q = q_0 = 5 \times 10^{-3}$ g/g $\quad Z < 1\text{km}$

$q = q_0 - 0.2 \times 10^{-5}(Z - 1000)$ g/g $\quad 1\ \text{km} < Z < 2\ \text{km}$

B: $\Theta = \Theta_0 = 305\text{K}$

$q = q_0 = 10 \times 10^{-3}$ g/g $\quad Z < 1\text{km}$

$q = q_0 - 0.4 \times 10^{-5}(Z - 1000)$ g/g $\quad 1\ \text{km} < Z < 2\ \text{km}$

The surface cooling rate is also taken to be $-1.0\ \text{Kh}^{-1}$, and the moisture at surface doesn't vary with time. The other conditions are similar to those discussed before.

Our numerical simulations indicate that the SBL can still approach the quasi-steady-state after introducing the long wave radiation if the constant surface cooling rate is used as the lower boundary condition. Fig.4 shows how longwave radiation of atmosphere influences the vertical distribution of $\overline{w'\theta'} / (\overline{w'\theta'})_0$. The profiles of $\overline{w'\theta'} / (\overline{w'\theta'})_0$. with radiation of atmosphere is quite different from those without radiation. In the lower part close to the surface, $\overline{w'\theta'} / (\overline{w'\theta'})_0$ increases with height and reaches the maximum at a certain height. Our simulation shows that this height is generally between 0.05 h and 0.1 h in the quasi-steady-state. Garratt (1981) also obtained the similar conclusion. The increase of $\overline{w'\theta'} / (\overline{w'\theta'})_0$ with height in the lower part of SBL indicates that the role of the turbulent transport in this region is to warm the SBL rather than to cool SBL as that without longwave radiation. In the middle and upper part of SBL, however, the radiative cooling decreases sharply with height and is relatively small. In order to maintain the nearly steady-state of SBL, the role of turbulent transport is to cool SBL. So, in this case the turbulent transfer plays two different roles in the different parts of SBL. But the longwave radiation of atmosphere always provides the cooling. From Fig.4, we can also see that the moisture has a little influence upon $\overline{w'\theta'}$ if SBL is in a non-saturation state.

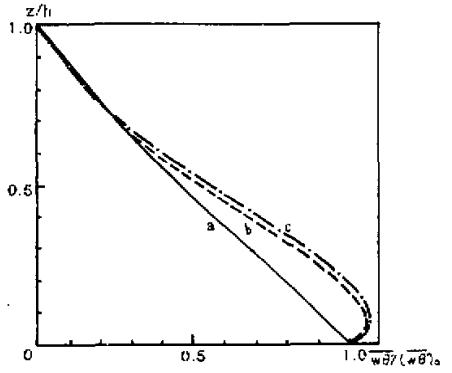

Fig.4. The normalized heat flux as a function of z/h when SBL approaches the "quasi-steady-state". Lines represent the simulated results of our model. a: without considering radiation of atmosphere. b: considering radiation of atmosphere with initial state B. c: considering radiation of atmosphere with intial state A.

Our numerical simulation also shows that the vertical distribution of τ, $\bar{e}^2$, $\overline{w'^2}$ have less changes comparing with those without radiation. This means that the longwave radiative cooling connects strongly with the mean and turbulent temperature fields, but is weakly related to the velocity fields. From the second-order turbulence equations (9)-(16), we can see that τ, $\bar{e}^2$, $\overline{w'^2}$ are coupled to temperature field only weakly through turbulent length scale l. Therefore, the longwave radiation influences the velocity field indirectly.

IV. CONCLUSIONS

In this study, we use a second-order turbulent model to simulate the formation and evolution of SBL, and discuss the influence of surface radiation cooling, terrain, baroclinicity and nocturnal long wave radiation upon the development of SBL. Besides, we emphatically analyse the structure and vertical distribution of the second-order turbulent moments. The simulation indicates that:

1. Under barotropic, flat terrain condition, if SBL is in the quasi-steady-state, the vertical dimensionless profiles of $\overline{w'\theta'}/(\overline{w'\theta'})_0$ and τ/τ_0 have little relation with the strength of radiative cooling of surface, and the exponent α_1 approximately equals 1. If SBL develops rapidly (e.g., in the evening transition after sunset), α_1 can be far larger than 1. One of the most significant reasons for the changes of turbulence fluxes of heat and momentum is the non-steady-state of SBL. The relation between α_1 and α_2 is also related to the developing state of SBL. In general, α_1 is larger than α_1 except the initial phase of SBL.

2. The exist of terrain can modify the vertical distribution of the second-order turbulent moments. The exponents $\alpha_1, \alpha_2, \alpha_e, \alpha_w$, and α_θ, decrease with the increase of slope.

3. Baroclinicity caused by cool and warm advections plays different roles in the distribution of second-order turbulent moments. The cool advection makes the distribution exponents larger, while the warm advection makes the exponents smaller.

4. Nocturnal longwave radiation plays a very important role upon mean and turbulent temperature fields in the lower part of SBL, and thus causes the variations of vertical profiles $\overline{w'\theta'}/(\overline{w'\theta'})_0$, $\overline{\theta'^2}/T_*^2$ in SBL. But this role has less influence upon turbulent velocity

fields.

5. A_e, A_w and A_θ are almost constant under different conditions. This means that in the surface layer a certain relation among second-order turbulent moments and u_*, T_* may exist. The constants A_e, A_w, A_θ are only determined by the nature of atmospheric turbulence itself. But at the present, we can not yet give the values of these constants exactly. We have to make a further study.

REFERENCES

Andre, J. C. De Moor, G., Lacarrere, P., Therry, G., and du Vachat, R: (1978), 'Modeling the 24-hour Evolution of the Mean and Turbulent Structures of the Planetary Boundary Layer', *J. Atmos. Sci.* **35:** 1861-1883.

Atwater. M. A. (1974), "The Radiation Model" Sect 4. Vol I CEM Rep. No.5131-4099, pp 67-82.

Blackadar. A. K. (1979), 'High Resolution Models of the Planetary Boundary Layer. Advances in Environment Science and Engineering. Vol.I No.1 J.Pafflin and E. Zieglar, Eds Gorchen and Breach, 50-85.

Brost. R. A, and J. C. Wyngaard (1978), "A Model Study of the Stably Stratified Planetary Boundary Layer" *J. Atmos. Sci* **35:** 1427-1440.

Caughey, S. J., Wyngaard, J. C. and Jaimal, J. C. (1979), "Turbulence in the Evolving Stable Layer", *J. Atmos. Sci.* **36:** 1041-1052.

Garratt. J. R. and R. A. Brost (1981), "Radiative Cooling Effects within and above the Nocturnal Boundary Layer" *J. Atmos. Sci.* Vol.38: 12 2730-2746.

Lascer and Arya (1986), "A Numerical Model Study of the Structure and Similarity Scaling of the NBL" Bound-Layer Meteor. **35:** 369-386.

Lenschow. D. H., li XingSheng, Cui Juan Zhu (1988), "The Stratified Boundary Layer Over the Great Plains" Bound-Layer Meteor. **42:** 95-121.

Li Xingsheng and Yang Shuowen (1986), "A Numerical Simulation of the Nocturnal Boundary Layer with Second-Order Model", Scientia Atmospherica Sinica, **10:** 154-163.

Li Xingsheng (1989), "On Similarity and the Turbulent Structure in the Stable Boundary Layer", *Acta Meteorologica Sinica*, **47:** 257-264.

Nieuwstadt. F. T. M (1984), "The Turbulent Structure of Stable Nocturnal Boundary Layer" *J. Atmos. Sci.* **41:** 2202-2216.

Richtmyer. R. D. (1975), "Difference Methods for Initial-Value Problems Intersience 283 pp.

Sorbjan. Z. (1986), "A Numerical Model Study of the Structure and Similarity Scaling of the NBL" Bound-Layer Meteor. **34:** 377-397.

Wyngaard. J. C. (1975), "Modeling the Plantary Boundary Layer Extension to Stable Case" Bound-Layer Meteor. *9:* 441-460.

Yamamoto. S., Yokoyama. O. etal. (1979), "Observational Study of the Turbulent Strcture of the Atmospheric Boundary Layer Under Stable Condition" *J. Meteor. Soc. Japan* **57:** 423-430.

Yokoama. O. etal (1979), "The Vertical Profiles of the Turbulence Quantities in the Atmospheric Boundary Layer" *J. Meteor. Soc. Japan*, **57:** 264-272.